TECHNICAL REPORT
NATICK/TR-92/032

AD _____

ANALYSIS OF BALLISTICALLY CAUSED DAMAGE IN SOME TEST PANEL FIBERS

SAMUEL H. COHEN
ROBERT A. PROSSER*
ABRAM KING
C. RICHARD DESPER**

May 1992

Final Report
October 1986 - September 1989

This report revises and replaces
NATICK/ TR-91/027, May 1991

UNITED STATES ARMY NATICK
RESEARCH, DEVELOPMENT AND ENGINEERING CENTER
NATICK, MASSACHUSETTS 01760-5000

SOLDIER SCIENCE DIRECTORATE
*INDIVIDUAL PROTECTION DIRECTORATE
**MATERIALS TECHNOLOGY LABORATORY, WATERTOWN, MA

DISCLAIMERS

The findings contained in this report are not to be construed as an official Department of the Army position unless so designated by other authorized documents.

Citation of trade names in this report does not constitute an official endorsement or approval of the use of such items.

DESTRUCTION NOTICE

For Classified Documents:

Follow the procedures in DoD 5200.22-M, Industrial Security Manual, Section II-19 or DoD 5200.1-R, Information Security Program Regulation, Chapter IX.

For Unclassified/Limited Distribution Documents:

Destroy by any method that prevents disclosure of contents or reconstruction of the document.

REPORT DOCUMENTATION PAGE

Form Approved
OMB No. 0704-0188

1. AGENCY USE ONLY (Leave blank)	2. REPORT DATE	3. REPORT TYPE AND DATES COVERED
	May 1992	Final Report - Oct 1986 to Sep 1989

4. TITLE AND SUBTITLE
Analysis of Ballistically Caused Damage in Some Test Panel Fibers

5. FUNDING NUMBERS
PE: 1L161102
PR: AH5202
WU: T/B1252
AGG CODE: T/B 1032

6. AUTHOR(S)
Samuel H. Cohen, Robert A. Prosser, Abram King and C. Richard Desper*

7. PERFORMING ORGANIZATION NAME(S) AND ADDRESS(ES)
U.S. Army Natick Research, Development and Engineering Center
Kansas Street, ATTN: STRNC-YSP
Natick, Massachusetts 01760-5020

8. PERFORMING ORGANIZATION REPORT NUMBER
NATICK/TR-92/032

9. SPONSORING/MONITORING AGENCY NAME(S) AND ADDRESS(ES)

10. SPONSORING/MONITORING AGENCY REPORT NUMBER

11. SUPPLEMENTARY NOTES
*C. Richard Desper, U.S. Army Lab Command, MTL, Watertown, MA

NOTE: This report revises and replaces NATICK/TR-91/027, dated May 1991.

12a. DISTRIBUTION/AVAILABILITY STATEMENT
Approved for Public Release, Distribution Unlimited

12b. DISTRIBUTION CODE

13. ABSTRACT *(Maximum 200 words)*

In this report we describe microscopic and X-ray diffraction methods to analyze ballistically induced damage to fibers and yarns within multilayer panels of Spectra-900 and Spectra-1000 polyethylene and Kevlar. Microscopic evaluation by scanning electron microscopy showed heat-induced damage in fibers several layers beyond the layer in which the .22-caliber projectile came to rest, and X-ray diffraction showed crystallinity differences in fibers close to and at some distance from the point of ballistic impact. Polarization microscopy was used to corroborate the X-ray diffraction findings, by elucidating differences in birefringence within the fibers.

14. SUBJECT TERMS
YARNS, FIBERS, BALLISTICS, BALLISTIC IMPACT, X-RAY DIFFRACTION, MICROSCOPY, ELECTRON MICROSCOPY, SCANNING, IMAGE ANALYSIS

15. NUMBER OF PAGES
51

16. PRICE CODE

17. SECURITY CLASSIFICATION OF REPORT	18. SECURITY CLASSIFICATION OF THIS PAGE	19. SECURITY CLASSIFICATION OF ABSTRACT	20. LIMITATION OF ABSTRACT
UNCLASSIFIED	UNCLASSIFIED	UNCLASSIFIED	UNLIMITED

TABLE OF CONTENTS

LIST OF FIGURES

LIST OF TABLES

PREFACE

The purpose of the project "Image analysis of ballistically caused damage along the fiber axis" (AH5202033) which was carried out from 1986-1989, was to investigate the type and extent of damage done to the fibers and yarns within ballistic panels subjected to the impact of 0.22 caliber projectiles. The results of the study, which utilized X-ray diffraction, electron and polarized light microscopy, and the interpretation of the results are given in this report.

This report is a revision of NATICK/TR-91/027, "Analysis of Some Ballistically Caused Damage in Some Test Panel Fibers." The value of 0.020% given in NATICK/TR-91/027 was incorrect. It was based on a incorrect constant obtained from Allied Fibers, Inc., over the telephone. The error arose in the course of converting from mixed English/metric units to metric units. The error is regretted.

The authors thank the following individuals for their suggestions and help: Mrs. Janet Ward and Mr. John Song of the Individual Protection Directorate, Ms. Colleen Kelley of the Soldier Science Directorate, Natick RD&E Center, and Dr. Joseph Prifti and Mr. James Mackowitz, U.S. Army Materials Technology Laboratory, Watertown, MA.

We also acknowledge and thank Mr. Philip Cunniff, Mr. Ronald A. Segars, and Mr. John Halliday for their constructive criticism and for the considerable amount of time and effort spent in reviewing and qualifying this report.

Citation of trade names in this report does not constitute an official endorsement or approval of the use of a product.

ANALYSIS OF BALLISTICALLY CAUSED DAMAGE IN SOME TEST PANEL FIBERS

INTRODUCTION

The objective of this report is to describe microscopic, X-ray diffraction and other methods used to elucidate the type and extent of ballistically induced damage to fibers within multilayered panels of Spectra 1000$^{(R)}$ cloth. Evidence that softening and melting of the yarns plays an important role in ballistic penetration will be presented.

Light microscopy (LM) was employed to evaluate internal features of each type of fiber prior to and following ballistic impact. In addition, polarized LM was used to observe morphological changes to those fibers subjected to X-ray analysis.

The surface features of each group of fibers were viewed using scanning electron microscopy (SEM), which provided a three-dimensional perspective of both fibers and yarns.

Transmission electron microscopy (TEM) was used in conjunction with ultramicrotomy in an attempt to obtain high resolution images of the ultrastructural morphologies of each type of fiber.

X-ray diffraction (XRD) analyses before and after impact were also performed on fibers close to and far away from the point of ballistic impact in order to ascertain variations in crystal structure (possibly due to heat effects) relative to the distance from the point of impact.

In recent studies (Prosser, 1988a,b) it was pointed out that the mechanism of penetration of ballistic panels by projectiles was uncertain, and that breaking of the yarns under tensile conditions was not necessarily the prime mode of failure of the yarns.

EXPERIMENTAL

BALLISTICS

Ballistic panels measuring 12" x 12" were prepared from stacked layers of cloth whose edges were fastened by sewing. The Spectra-1000 cloth was style 952, 6 oz/yd^2, plain weave, 33 warp x 33 filling, 650 denier, scoured. It consisted of ultra-high-density, high-molecular-weight, highly crystalline polyethylene fibers. A detailed account of firing conditions can be found in Prosser (1988a).

MICROSCOPY

Light microscopy (LM), scanning electron microscopy (SEM), transmission electron microscopy (TEM), and X-ray diffraction were all employed in this project for the purpose of evaluating the morphological characteristics of fibers and yarns obtained from ballistic panels that had been penetrated by a 0.22-caliber projectile.

For LM a Zeiss Ultraphot camera microscope was used. Individual or groups of fibers cut from panel cloth were mounted onto glass slides under coverslips affixed to the slides with tape. The coverslips helped to protect and hold down the fibers. A variety of objective lenses were used to vary the magnification and Polaroid types 52 and 55 film were used for photography.

A Zeiss CSM 950 was used for SEM. Fibers or yarn were affixed to an aluminum stub with double-sided sticky tape, sputter coated with AuPd and then inserted into the SEM's specimen chamber. Photomicrographs were taken with Polaroid type 52 film.

For TEM sample preparation, fibers and yarns were cut into 5 mm lengths and placed into wells of a glass specimen culture plate containing approximately 15 drops of Spurr's low viscosity resin mixture for one hour. While this step was being carried out, individual block compartments of a silicon rubber mold were partially filled with the resin mixture.

The samples from the culture plate were then transferred to the mold and some additional resin added. A fine needle was used to properly orient the samples within each block and to puncture any air bubbles which appeared. Next, the mold containing up to 21 samples was placed in an oven set at 70°C for 48 h to cure.

Once the blocks had hardened they were removed from the oven, trimmed and sectioned (cut into slices) to a thickness of 30-40 nm with a Sorvall MT2B Ultramicrotome having a glass knife. The thin sections were then picked up onto 3 mm/175 mesh Cu grids and the samples within the sections were viewed with a Hitachi 600-2 TEM and photographed with Kodak SO163 Electron Image film.

X-RAY DIFRACTION

X-ray diffraction analysis was conducted for 16 Spectra-1000 test panels. Spectra 1000 is an ultra-high-density, high-molecular-weight semicrystalline polyethylene fiber with orthorhombic and monoclinic crystals. Crystalline content was determined twice for each panel--once adjacent to the point of impact, and a second time at an undamaged area distant from the impact point. Changes in crystallinity indicate substantial heat effects.

The following diffraction peaks were observed: the monoclinic (001) reflection, near $2\theta = 19.4^{\circ}$; and the orthorhombic (110) and (200) reflections, near $2\theta = 21.5^{\circ}$ and 23.8°, respectively. In every instance the equilibrium crystal form, the orthorhombic, predominated, as evidenced by the strength of the peaks at 21.5° and 23.8°. The metastable monoclinic phase comprised a minor fraction of the crystalline material when it was present.

The monoclinic phase of polyethylene has been observed by a variety of workers: Slichter (1956); Seto et al. (1962, 1968); Magill et al. (1965); Fatou et al. (1965), and Mead et al. (1979). In general, monoclinic materials appear as the result of cold-working of polyethylene, e.g., by compression or shear below the crystalline melting point. The monoclinic phase is generally thought of as a metastable phase, less stable than the orthorhombic phase, to which it will spontaneously transform under favorable conditions, such as heating near the melting point or removal of applied stress. The polymer molecular weight also plays an important role: higher molecular weights favor the formation of the monoclinic phase.

The X-ray diffraction data were acquired using a specially modified Picker four-circle X-ray diffractometer, as described by Desper (1986). The system consists of the X-ray diffractometer, a PDP-11/23 computer for control of the four diffractometer angles: phi-crystallite orientation angle in fibers; chi-orientation within the fiber axis, which is redundant and is zero; omega-orientation of incident X-ray beam on sample; and two theta-Bragg diffraction angles. A position-sensitive proportional counter, and a multiple channel analyzer were used for data acquisition and presentation. Determination of crystallinities of fibrous materials presented a special problem, however, since the preferred crystallite orientation in the fibers results in a complicated diffraction pattern dependent upon both the usual Bragg angle 2θ and the fiber orientation angle X. This problem was overcome by averaging out the orientation effect on the diffraction instrument to reduce the data to patterns dependent upon only the angle 2θ, to which established methods for unoriented samples could be applied.

The X-ray beam has a circular cross-section diameter of 0.5 mm and, at a monochromatic wavelength of 1.54 angstroms, is capable of penetrating the thickness of the small areas in the test panel without serious absorption effects. Thus, the effective sample is a cylindrical section of fabric of 0.5 mm diameter, and of height equal to the fabric thickness. The beam diameter is considerably larger than the fiber yarn diameter but smaller than the .22-caliber projectile size. In all undamaged zone patterns, the target area of the X-ray beam was placed an inch from the damaged zone and not along a warp or woof line through the point of impact. Damaged zone patterns were taken by placing the beam on fabric material as close as possible to the point of ballistic impact.

The raw data were also adjusted for a Lorenz-polarization correction, which involves the diffraction instrument geometry and its systematic effect on measured intensities as a function of the Bragg angle 2θ.

RESULTS AND DISCUSSION

BALLISTICS

In the study of the ballistic performance of flexible armor, there appear to be three main factors: tensile strength of the yarns, shear strength of the yarns, and, because there is so much evidence of it for some materials, melting. The first two were addressed by Prosser (1988 a,b) who showed that tensile failure appeared to be of minor importance, and that the primary mechanism of penetration was probably shearing. Since much of the literature predicates ballistic behavior on tensile properties, this report again investigates the problem of the relative importance of tensile versus shear strength. Also, the role of softening and melting of the yarns due to frictional heat will be explored.

When a projectile penetrates a cloth ballistics panel, the kinetic energy absorbed appears to be distributed over four energy sinks: 1. The energy needed to stretch the yarns. 2. The energy absorbed in shearing the yarns. 3. The energy absorbed by the cloth when the layers are distended into a cone by the projectile before penetration of each layer (cone formation). 4. Heat. The assumption is made that there are no other significant energy sinks in a projectile-ballistic panel system.

First the behavior of the panels under quasi-static (the usual) laboratory conditions and at ballistic velocities will be compared and differences noted. A rationalization of these differences will then be offered.

In studying the penetration of a textile ballistic panel, one would expect that the force and work of penetration for a sharp projectile would be much less than for a blunt projectile. To test this hypothesis, three types of projectiles were used. All were .22-caliber, with flanges, had different leading surfaces, and had the same mass, 17 grains $\pm$ 1%. One projectile was simply a right circular cylinder (RCC) with a flange, i.e., the leading surface was flat, perpendicular to the axis of the projectile, and consequently made a 90^{o} angle with the cylindrical side. Although the leading surface is quite flat and therefore would be considered blunt, nevertheless, because of its ballistic performance (discussed below), the RCC is considered to be very sharp. The blunt projectiles were simply RCC's with the 90^{o} edge substantially rounded, but not enough to make the leading surface hemispherical. The third type of projectile was the 0.22 caliber fragment-simulating projectile (FSP), which is the standard projectile used in evaluating the performance of flexible armor. Figure 1 shows all three projectiles.

Figure 2 is a schematic of a 0.22-caliber FSP. One side view presents a rectangle; the other shows a truncated wedge (the slope of the two sides that intersect the flat rectangular surface is 55^{o}). The behavior of the FSP was expected to fall between that of the sharp and blunt projectiles because on the one hand the FSP has 90^{o} edges (two), similar to the sharp

projectile, and on the other it has 55° edges (two), which should have a rounding effect (compared with the 90° edge) making the penetration similar to that of the blunt projectile.

To test the hypothesis that the ballistic behavior of these three styles of projectile leading surfaces at ballistic velocities will parallel their behavior at quasi-static velocities, as provided by laboratory tensile testing apparatus, steel bars, as shown in Fig. 3 (Prosser, 1988b) were prepared. They were 6" x 1" x 1/4" and could be fastened in a holder, also shown. The holder was inserted into the upper jaw of the tensile testing apparatus. The yarn was then looped over the bar A (the horizontal round control bar), both ends inserted into the lower jaw and the breaking tenacity determined. One of these bars (B) was rectangular, i.e., the edges were all 90°. This bar then corresponded to the RCC projectile. The rectangular bar also represented one side view of the FSP. A third bar (C) was prepared by taking a rectangular bar and chamfering two of the 90° edges at 55° as shown in Fig. 3. This bar then represented the other side view of the FSP. So now we had sharp, intermediate (FSP), and blunt projectiles and the analogous bars. Additional bars with apex angles of 150° (D), 120° (not shown), 90° (E), and 60° (F) were also prepared for comparison purposes.

It was found (average of 10 or more determinations) that the tensile strength in grams/denier for yarns of Spectra 1000(R), Spectra 900(R), and Kevlar 29(R) when looped over the rectangular bars (one side view of a FSP) was less than half that when looped over the bar with 55° edges (the FSP's other side view), and much less than that when looped over the cylindrical (blunt) bar. The results for these three bars and bars with apex angles of

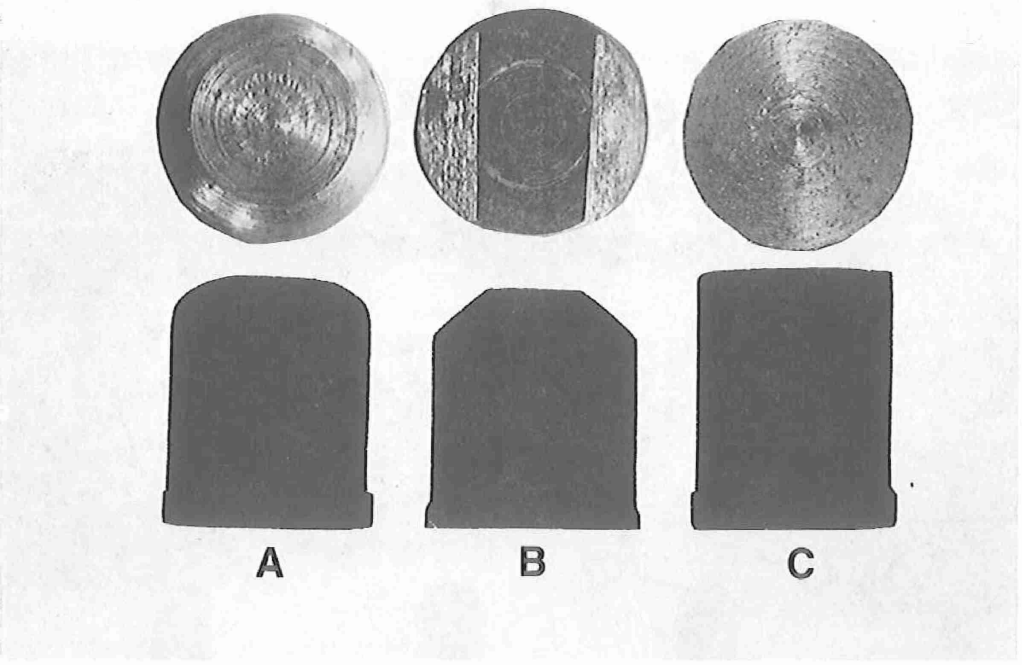

Figure 1. Three Types of Projectiles: A. Blunt; B. Fragment Simulating; C. Sharp

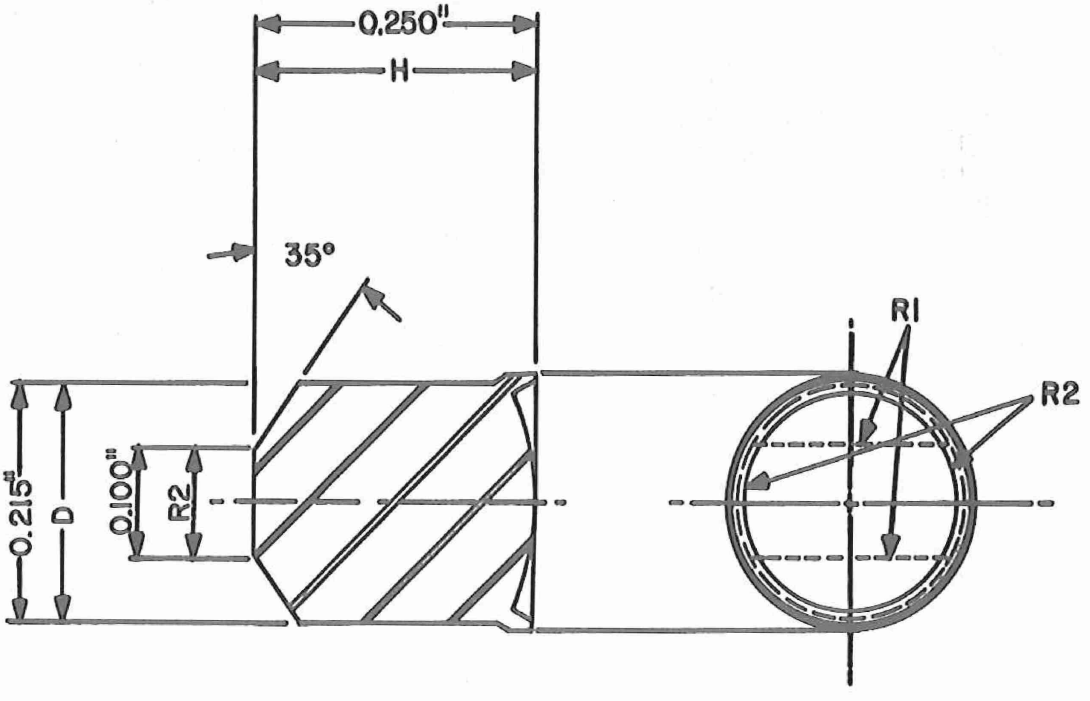

Figure 2. Fragment Simulating Projectile, Caliber .22, Steel

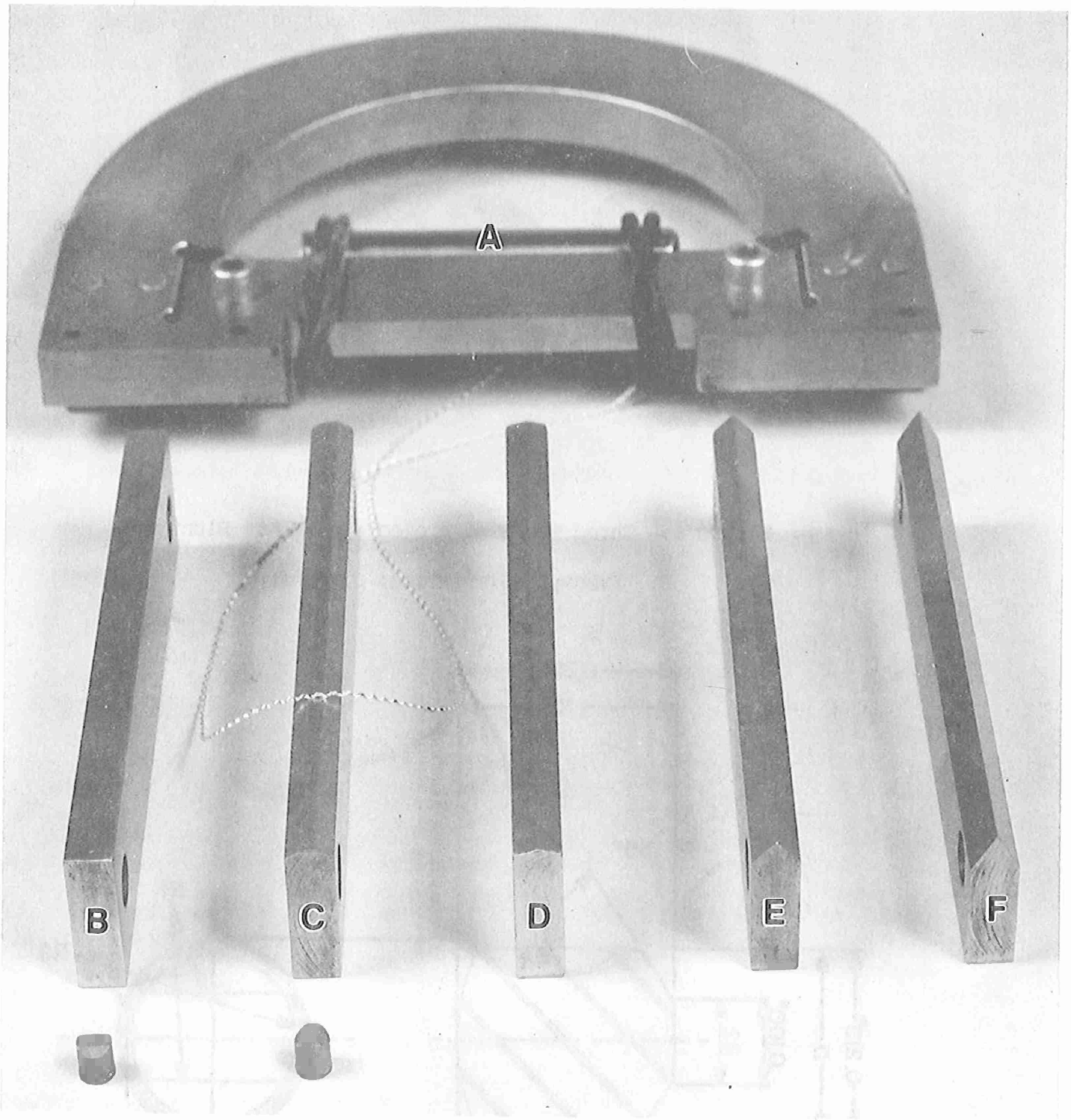

Figure 3. Steel Bars and Holder for Testing.

150^{o}, 120^{o}, 90^{o}, and 60^{o} are plotted in Fig. 4. Since the breaking tenacity over the rectangular bar was the least in all cases, the rectangular bar behaved as if it were the sharpest despite the fact that it appeared to be the bluntest.

Examination of failed yarns showed that, for the round bar, the filaments broke at random over a considerable length of the yarn. For the others, practically all of the filaments broke at one or more edges of the bar. In some cases all the filaments failed at one spot as if the yarn had been cut. Apparently, shearing is involved in the mechanism of failure. If failure were entirely due to exceeding the tensile strength of the yarns, these plots would all be horizontal lines. The shape of the surface over which the yarns are broken is important - under quasi-static conditions, i.e., low strain rates. Similar results were obtained for nylon (Prosser, 1988b).

Consequently, at ballistic velocities, it would not be surprising to see, on a qualitative basis, that a blunt projectile (analogous to the round bar) required much more energy per layer to penetrate a ballistic panel than a sharp projectile, the RCC (analogous to the rectangular bar). The energy per layer required by an FSP, which has sharp edges (the 90^{o} edges) as well as a more rounded surface (over the 55^{o} edges), should fall somewhere between the two.

Two sets of eight Spectra-1000 ballistic panels having 2,6,13,19,25,30, 35, and 40 layers were fired using the sharp projectiles for one set and the

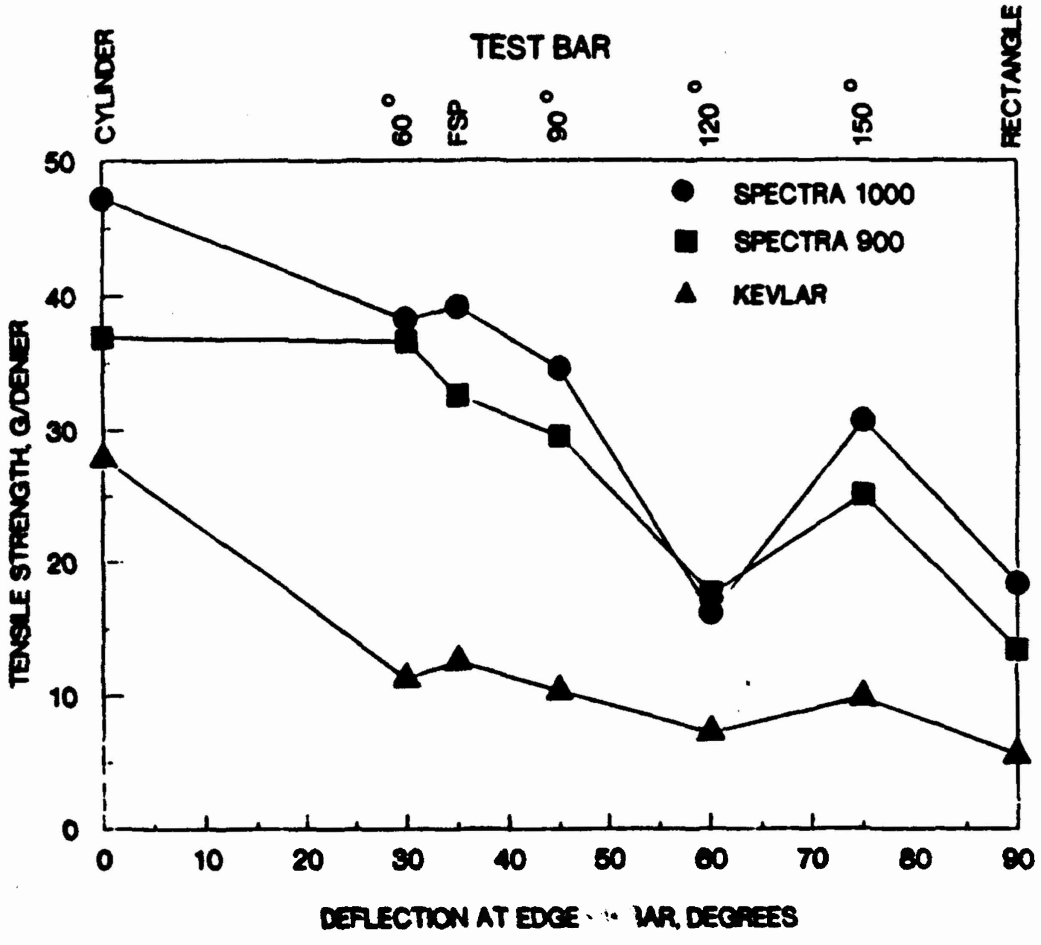

Figure 4. Plots of the Tensile Strength of Spectra 1000, Spectra 900 and Kevlar 29 Using Different Test Bars

TABLE 1

Firing Data for Spectra-1000 Ballistic Panels
Using Blunt, Sharp and FSP Projectiles
(.22-caliber, 17 grains, fired at zero degrees obliquity)

Style of Projectile	Number of Layers In Panels	Areal Density g/m^2	V_{50} ft/s	V_{50} m/s
Blunt	2	420.7	699	213.1
Blunt	6	1228.0	969	295.4
Blunt	13	2601.7	1348	410.8
Blunt	19	3862.0	1384	421.8
Blunt	25	5054.1	1706	520.0
Blunt	30	6201.8	1755	534.9
Blunt	35	7122.2	1874	571.1
Blunt	40	8367.4	2029	618.4
Sharp	2	412.4	873	266.1
Sharp	6	1234.5	1079	328.9
Sharp	13	2710.6	1333	406.3
Sharp	19	3977.4	1541	469.7
Sharp	25	5155.6	1806	550.5
Sharp	30	6166.7	1961	597.7
Sharp	35	7268.3	2034	620.0
Sharp	40	8215.0	2203	671.5
FSP	2	417.4	777	236.8
FSP	5	1038.3	1004	306.6
FSP	10	2068.2	1284	391.4
FSP	15	3054.8	1429	435.6
FSP	20	4110.7	1591	484.9
FSP	25	5174.2	1721	524.6
FSP	30	6153.1	1928	587.7
FSP	35	7158.6	2026	617.5
FSP	40	8230.3	2195	679.4

blunt projectiles for the other. Another set of panels with 2,5,10,15,20, 25,30,35, and 40 layers was fired using FSPs. The path of the projectiles was perpendicular to the panel, i.e., the striking obliquity was zero.

V_{50} determinations were then obtained for all panels (Table 1), and plots of V_{50}^2 versus the number of layers of cloth in the ballistic panel were made (Fig. 5). The V_{50} is that velocity at which half of the projectiles are expected to penetrate the panel. Since the kinetic energy is given by $1/2\ (mV_{50}^2)$, where m is the mass of the projectile, the slope of the lines (Fig. 5) is proportional to the energy of penetration per layer (Prosser, 1988a) as seen by the projectile. The plots show that on a statistical basis (2 sigma), the energy of penetration per layer for the sharp and FSP projectiles is the same, whereas it is less for the blunt projectile. The straight line statistics are given in Table 2. (Since the ballistics performance of the RCC (sharp) and the FSP projectiles is essentially the same, one might as well use the former as the standard. They are easier to make, and, probably, cheaper.)

TABLE 2 Straight Line Statistics,
Projectile, Energy of Penetration/Layer

PROJECTILE Style	COEFFICIENT Value	95% CONFIDENCE INTERVAL Lower	Upper	R'*
Blunt Slope	0.881 X 10**4	0.785	0.975	0.994
Intercept	2.543 X 10**4	0.190	4.897	
Sharp Slope	1.004 X 10**4	0.931	1.007	0.997
Intercept	4.412 X 10**4	2.597	6.227	
FSP Slope	0.992 X 10**4	0.936	1.048	0.998
Intercept	4.137 X 10**4	2.809	5.464	

*R' is the coefficient of correlation

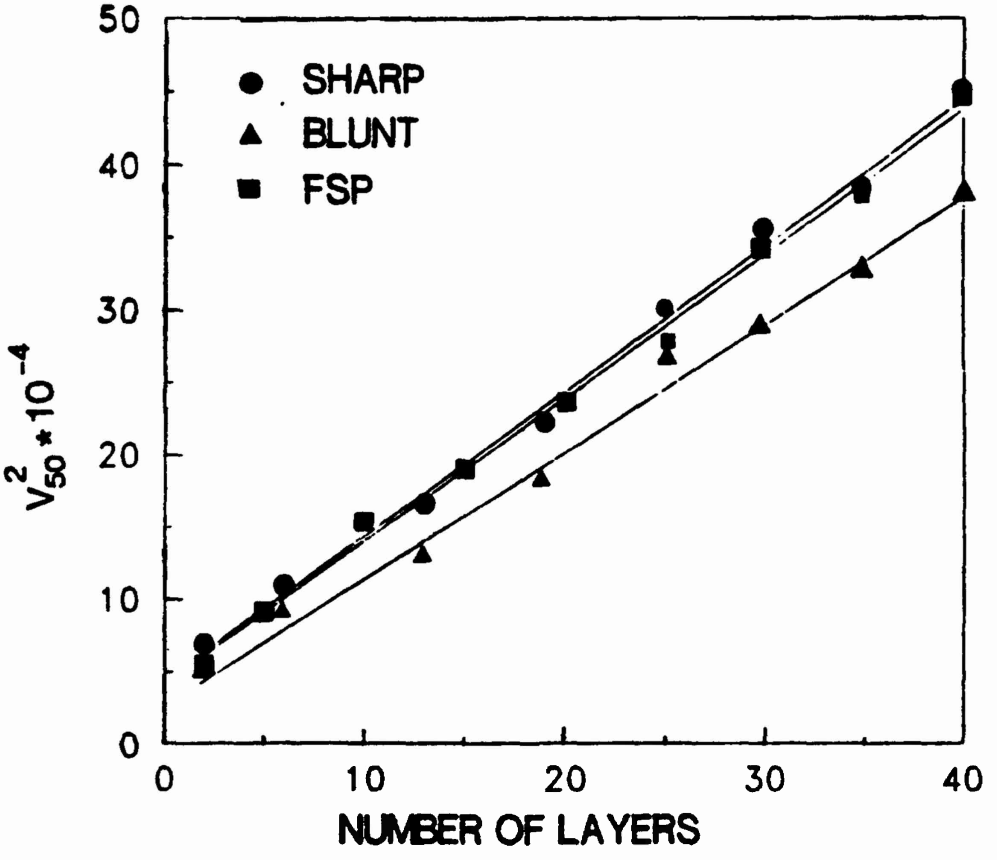

Figure 5. Plots of V_{50}^2 values vs. layers of cloth in ballistic panels for A. Blunt, B. FSP and C. Sharp projectiles.

If the distance over which the work is done is roughly the same for all three projectile styles, one estimates that the forces involved in penetrating the Spectra-1000 panels are in the same order as the work done by the three projectiles. Since the work of penetration per layer was practically the same for all three projectiles, so are the forces. There appears to be a discrepancy in that there is no qualitative agreement between the forces involved at quasi-static (Fig. 4) and at ballistic velocities (Fig. 5).

Instead of comparing the forces involved in the two cases (quasi-static vs. ballistic velocities), we can compare the work-to-break (toughness) values. Under quasi-static conditions, since the tensile strengths at break show large differences (See Fig. 4) and the shape of the stress-strain plot for Spectra-1000 is fixed, there should be large differences in breaking toughness values which parallel the tensile strength values. On the other hand, the differences in energy loss per layer for the three styles of projectiles were not large and were in a different sequence. Based on these observations, it was concluded that the differences in behavior under quasi-static and ballistic conditions could be real and not due to statistical variations from unknown causes.

In order to comprehend this anomalous result, we examined the fired ballistic panels in more detail. The number of yarns which failed in seven projectile holes within three ballistic panels were counted under a microscope (Table 3). Partially severed yarns were estimated to a tenth of a yarn. The corresponding energies of penetration were then calculated by subtracting the kinetic energy of the projectile after it exited the

panel from its kinetic energy when it struck the panel. The initial and final velocities were obtained at the time the V_{50} values were determined. The energies of penetration were then divided by the broken yarn values to obtain the energy attenuation per yarn, which was then corrected for denier (650).

TABLE 3

Energy Absorbed per Broken Yarn for .22-Caliber Blunt, Sharp, and FSP Projectiles Using Spectra 1000 Ballistic Panels

Hole #	Number of Layers in Panel	Number of Layers Penetrated	Projectile Style	Energy Loss J/broken yarn	Energy Loss J/denier
1	19	19	Sharp	1.46	2.25×10^{-3}
2	19	19	Sharp	0.70	1.08×10^{-3}
3	19	19	Blunt	1.18	1.82×10^{-3}
4	19	19	Blunt	1.68	2.58×10^{-3}
5	35	30	FSP	1.67	2.57×10^{-3}
6	35	33	FSP	1.69	2.60×10^{-3}
7	35	35	FSP	0.73	1.12×10^{-3}
			Average of three Projectile Styles		2.0×10^{-3}

The breaking toughness value of Spectra-1000 yarns under quasi-static conditions was obtained from Allied Fibers Corp., the manufacturer, and is 5.39×10^{-3} J /(denier M). Since the ballistic panels are one foot square (0.3048 x 0.3048 M), the maximum energy which can be absorbed by 12 inches of yarn would be 5.39×10^{-3} J x 0.3048 = 1.64×10^{-3} J. Therefore, for each yarn broken, the maximum toughness at quasi-static strain rates is 1.64×10^{-3} J.

However two additional adjustments must be made before the values obtained under ballistic and laboratory conditions can be compared. Under ballistic conditions there is substantial cone formation, and this requires additional energy. This energy decreases as the striking velocity reaches the critical velocity of the yarns and consequently of the cloth. By definition, the critical velocity is the striking velocity at which translation of the severed ends of the yarn in the direction of the projectile is negligible. One might define the critical velocity of the cloth similarly. The worst case, low striking velocity, is assumed in this case.

Correcting for cone formation so that only the tensile work-to-break (toughness) energy is involved under ballistic conditions would decrease the calculated value of 2.0×10^{-3} J by roughly 25%. The other correction is for the fact that under laboratory conditions, the entire length of yarn is equally stressed whereas under ballistic conditions this is definitely not the case. Examination of fired ballistic panels indicates that most of the energy of penetration is absorbed within about a one-inch radius of the hole. (A reason is given below.)

Correcting for the difference in yarn lengths involved under ballistic and laboratory conditions to a two-inch diameter basis would decrease the work-to-break energy absorbed under laboratory conditions by a factor of 6 (since the panel is 12 inches wide). The values, corrected for cone formation and active length (2 inches) of yarn, would be 1.5×10^{-3} J under ballistic conditions versus 0.27×10^{-3} J under laboratory conditions. The ratio is 1.54/0.27 = 5.6. Since the value under laboratory tensile conditions is the maximum energy that the yarns can absorb under

tensile conditions, we tentatively conclude that there is another energy sink involved which is not negligible. We postulate that this additional sink is heat which is generated by friction between yarns, between filaments within a yarn, and between fibrils within a filament. There may be direct conversion of kinetic energy to heat by compression of the air, compression and deformation of the filaments, as well as frictional effects.

The work of shearing would also be an energy sink. On examination of the holes in a ballistic panel under a microscope, it was found in many cases for both Spectra-1000 and nylon panels that all of the severed ends of the filaments in a yarn were on a smooth surface, in some cases, a plane. The ends of the filaments had remained on a surface because the material at or near the surface had fused together. The fact that the filament ends were all on the severed surface of the yarn indicates failure by shear through softened yarn. Consequently, it is difficult to assess the importance of shear and toughness as energy sinks.

The breaking-toughness values obtained at ballistic velocities are inherently and substantially different from the values obtained at low strain rates, due primarily to differences in the viscoelastic behavior of the polymer at the two velocities. This fact is not being disputed; however, a ratio less than unity was expected instead of 5.7.

Stress/strain curves generally, and those for nylon in particular (Fig. 6), at higher rates of strain have steeper initial slopes than at lower rates of strain (Smith et al., 1963). The tenacities are usually higher, but the breaking elongations may be equal to or less than the values obtained in the laboratory using a stress strain apparatus at conventional

rates of testing, depending on the nature of the material. Because of the uncertainty of breaking elongation, toughness values obtained at high strain rates using single yarns may be greater or less (but usually less) than those obtainable at conventional strain rates. Curve A of Fig. 6 was calculated from single yarn nylon data obtained at ballistic velocities. The area under the solid line portion of this curve is the breaking toughness, i.e., the energy required for yarn failure at ballistic velocities. It is certainly not in the order of 5.7 times the area under curves C, D, or E, the toughness at quasi-static strain rates. Plots for Spectra-1000 or Spectra-900(R) similar to Fig. 6 for nylon are not available. However, it is likely that other polymeric yarns, such as Spectra-1000, will show similar behavior, i.e., the area under the Spectra-1000 curve corresponding to curve A will not be in the order of six times the area of the curve corresponding to curves C, D, or E. Apparently an inconsistency which remains to be clarified exists between the quasi-static and ballistic results.

If one loosens the end of a yarn near the middle of an edge of a fired ballistic panel and pulls on it, one finds that it takes very little effort to duplicate the strained appearance of the yarns that were broken by the projectile. Usually the yarn does not break but simply slides out of the panel. If one teases a yarn from an edge of the cloth and tries to break it by hand, one finds that considerably more force is required. For the fifth and sixth holes (Table 3), the projectile stopped within the panel. Since the final velocity was zero, many of the yarns were stretched at quite low strain rates. In V_{50} determinations the exiting velocity is always low. One should find, in these cases, occasionally, that the original yarn ends

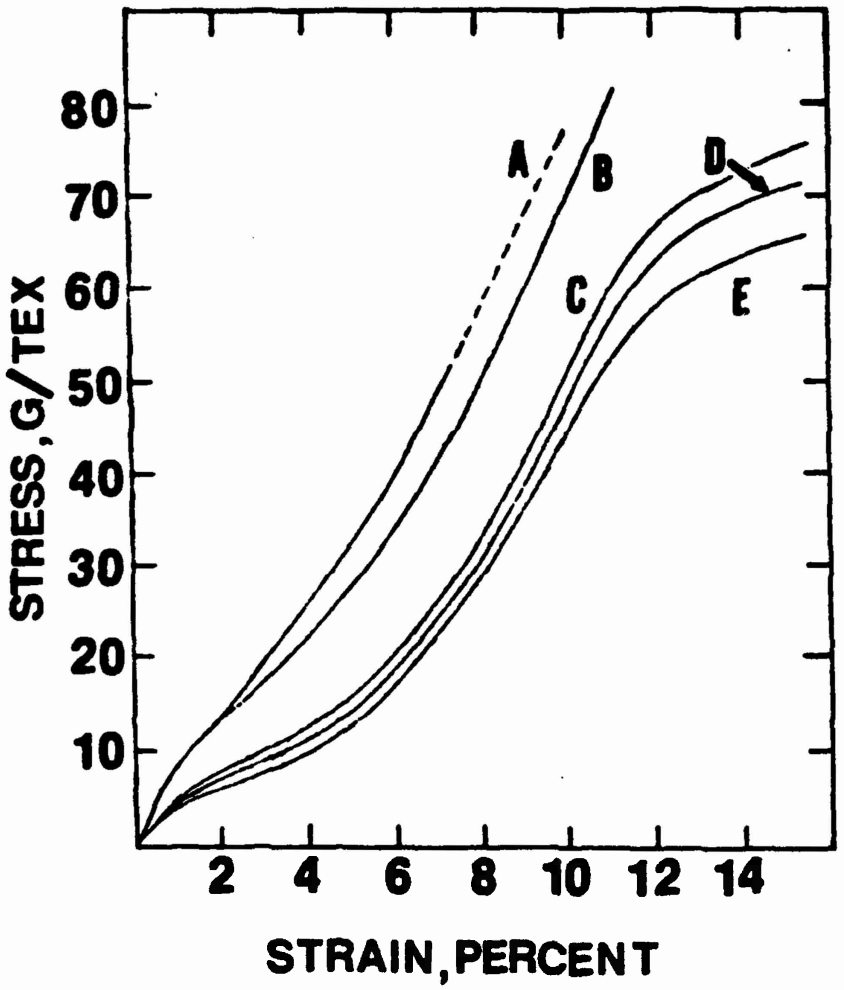

A. Ballistic Velocity (calculated from vertical transverse impact velocity and transverse wave front velocity)

B. 290,000% per min

C. 100% per min

D. 10% per min

E. 1% per min

FIGURE 6. Plots of stress vs. strain for nylon yarn at different rates of strain. Drawn from data by Smith et al. (1963). Reprinted by permission of the Textile Research Journal.

at the edges of the panel had been pulled inward past the cross yarns toward the hole (and remained there) despite the fact that the panel was clamped in place. We have never observed this. (A single Spectra-1000 yarn even when held in the pneumatic jaws of a tensile testing apparatus often slips when stressed.) Apparently the force exerted by the projectile to rupture a yarn is much lower than that required to break it manually. This difference would indicate that the strength of the yarns under ballistic conditions had decreased. This behavior appears to hold for nylon and Kevlar panels also.

When the broken Spectra-1000 yarns were counted under the microscope (Figs 7 and 8), the effects of heat were quite evident. This was also true for nylon. Heat, therefore, could be a major factor in the mechanism of penetration. So far its role does not appear to have been clarified. The possibilities are that melting could have occurred after the projectile reached a given interior layer and during or before penetration of that layer. The work of stretching the yarns would not appear as heat after the yarn was broken. On retraction, yarns cool. The projectile could be at an elevated temperature because of heat derived from its passage through the gun barrel, the air prior to striking the panel, and friction with prior layers of cloth. In the case of complete penetration of the panel, transfer of sufficient heat by conduction from the projectile to the cloth during their very brief encounter so as to account for the copious amount of resolidified polymer evident under the light microscope does not appear reasonable. Consequently, conduction of heat from the projectile to the yarns does not appear to be a major factor.

The third possibility is that the yarns of the interior or final layers of cloth were softened, at least superficially, to some extent prior to the

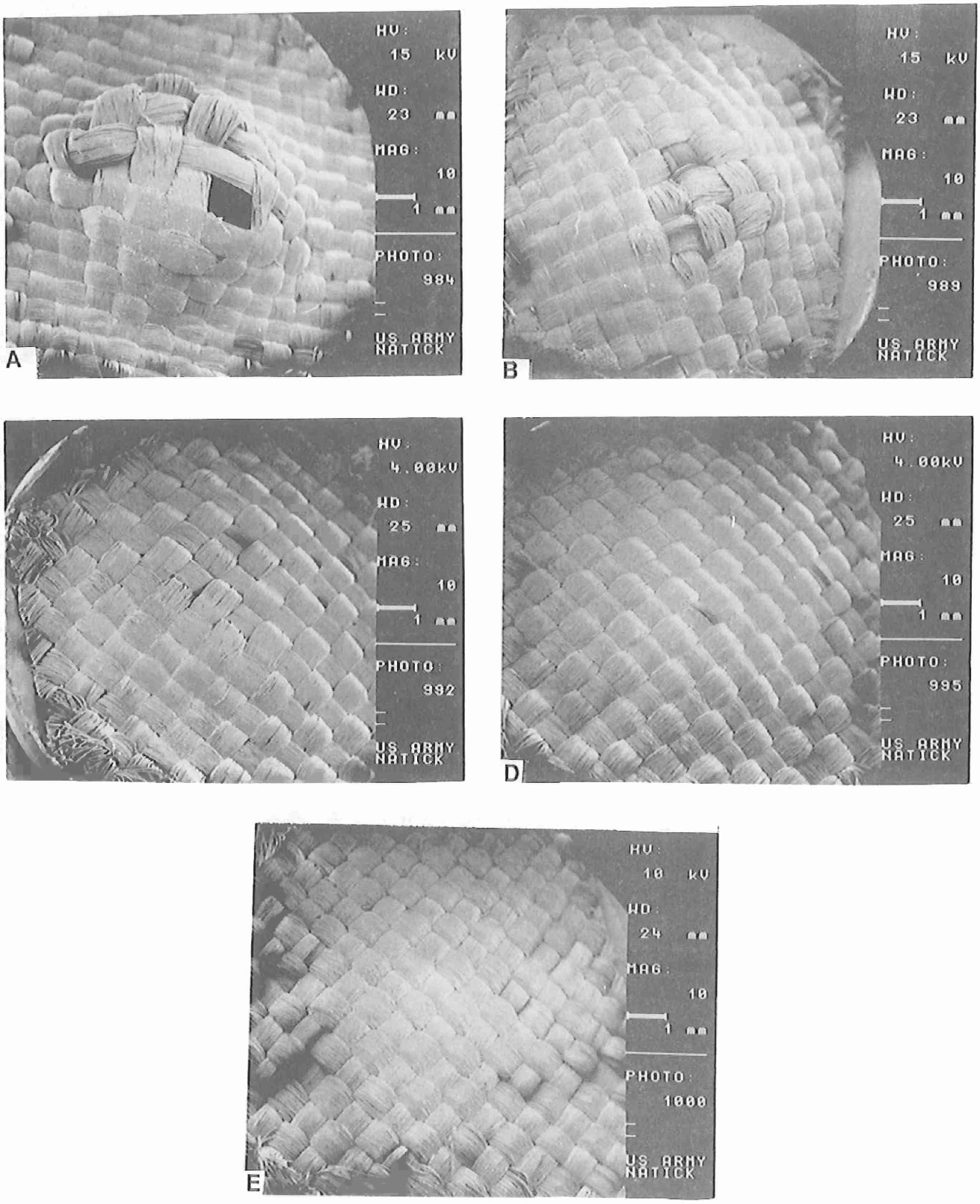

Figure 7. Scanning electron micrographs of Spectra-1000 ballistic panel yarn layers ahead of the layer in which the projectile stopped. A. First layer ahead. B. Second layer ahead. C. Third layer ahead. D. Fourth layer ahead. E. Fifth layer ahead.

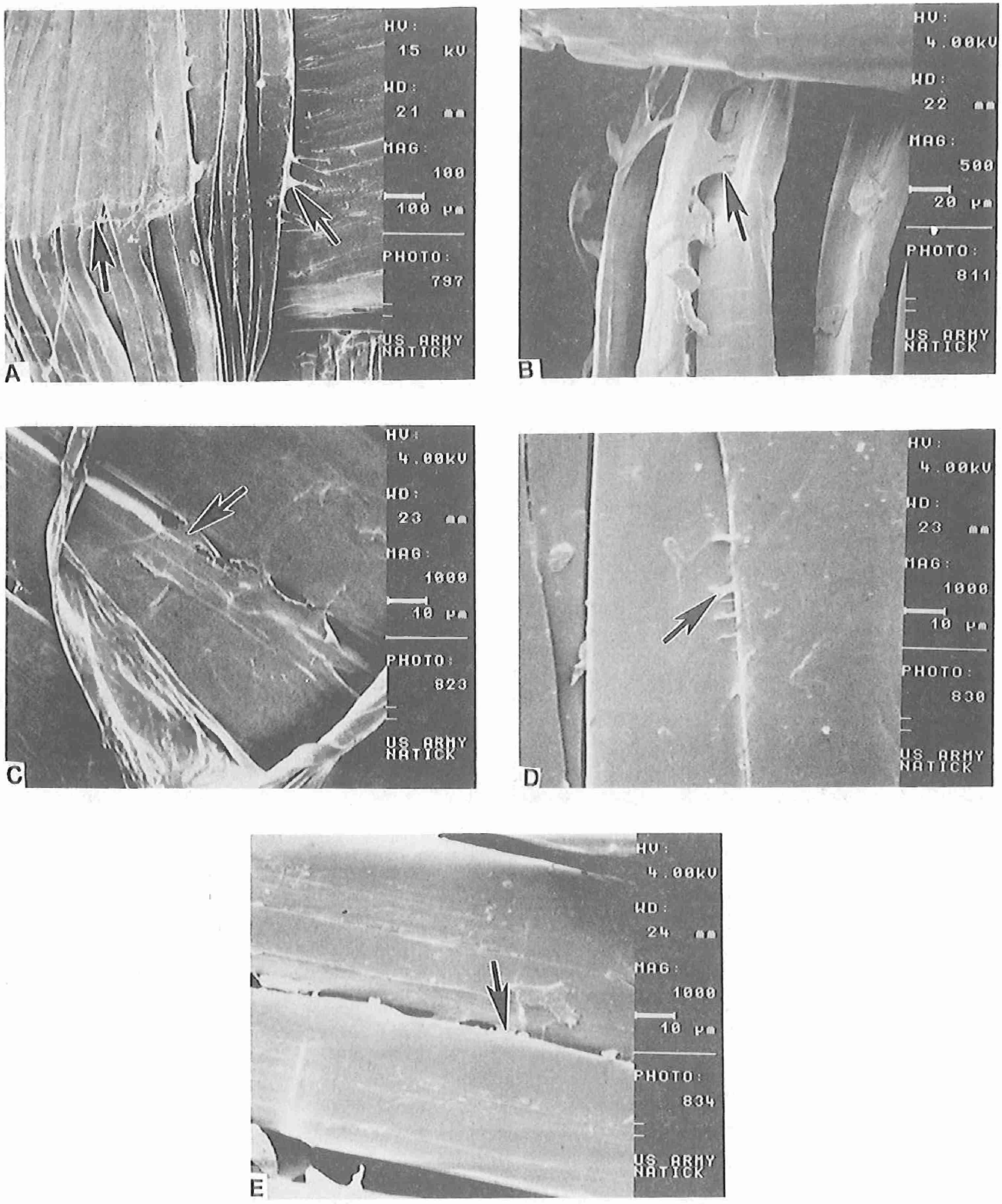

Figure 8. Spectra-1000 - Scanning electron micrographs of melted polymer bridges (arrows) in five layers of Spectra-1000 ballistic panel yarns ahead of the layer in which the projectile came to rest. A. First layer ahead of projectile. B. Second layer ahead. C. Third layer ahead. D. Fourth layer ahead. E. Fifth layer ahead.

arrival of the projectile. This might happen in the following manner: When the projectile strikes the panel, a shock (compressive) wave is transmitted ahead of the projectile. This puts considerable pressure on the yarns. Due to cone formation, which is concurrent, these yarns (filaments, fibrils) are forced to slide quickly past each other, and, since they are under high pressure, considerable frictional heat is generated. This can happen in many layers preceding the projectile. To ascertain this, a panel with a projectile arrested about half way through was examined. When layers of cloth immediately ahead of the projectile were viewed under a scanning electron microscope, numerous small bridges of resolidified polymer between filaments were found. Since sufficient frictional heat was generated to melt the surface of the filaments, it is reasonable to expect that larger amounts were softened. Photographs of these polymer bridges in five layers ahead of the layer where the projectile stopped are shown in Figs. 7 and 8. Since the amount of polymer in the bridges is small, the effects of heat may or may not be significant at low velocities. However, at high velocities the situation is quite different. Examination of a hole in a Spectra-1000 panel of 40 layers left by a sharp projectile showed that all of the layers of cloth in a cylinder within a radius of about 0.5 inches from the hole had completely fused together. The hole was rather smooth; there were few broken yarns in the hole. One could see through the hole. This happened, however, at high ballistic velocities. The striking velocity was 3524 feet/s and the exiting velocity was 2941 feet/s (896.4 meters/s). Since the panel was less than two centimeters thick, the transit time based solely on the exiting velocity was less than 25 microseconds. In another panel of 40 layers of Spectra-1000

cloth, this time penetrated by a blunt projectile, the result was practically the same including the transit time. Apparently, most of the kinetic energy is absorbed within a one inch-radius of the hole.

Evidence from XRD analyses presented later in this report shows that the morphological changes were more than superficial. Also, polarized light microscopy, discussed below, does show substantial morphological changes within filaments of yarns in the path of the projectile and ahead of the panel layer where the projectile stopped. However, the X-ray diffraction evidence provides no indication as to the source of the heat nor how and when it was generated and/or transmitted to the yarns.

Whether heat is or is not a major factor depends largely on the extent to which it is useful in elucidating ballistic phenomena, i.e., the extent to which it explains the apparently inconsistent or abnormal behavior presented above.

Since the cloth in the ballistic panel ahead and in the path of the projectile had been softened prior to its arrival as described above, one would expect the shape of the leading surface of the projectile to have little effect on the energy absorbed per layer. Fig. 5 shows this to be the case. Although the slope of the line (energy absorbed per layer of cloth) for the blunt projectile is statistically less than the slopes of the sharp and FSP projectiles, the difference is not that great considering the fact that the extremes of bluntness and sharpness are involved. Slippage of the yarns from in front of the blunt projectile would be the greatest of the three, and alone could account for the difference in slope. The differences in slopes are certainly much less than one might expect based on yarn

behavior at quasi-static strain rates (Fig 4), where heat effects prior to yarn failure are minor.

Softening would considerably diminish the tensile strength and therefore the toughness of Spectra-1000 and any other yarn. Only a very short length of yarn need be affected to result in premature failure. Another implication of the softening is that very little energy would be transmitted to the yarns in the fired panels, since it is difficult to transmit a tensile force through softened polymer. Consequently, very little manual effort would be required to duplicate the appearance of the yarns that were strained by the projectile in the cloth.

There are two other important ramifications of the softening/melting phenomena. The first is the linearity of the plots in Fig. 5. The linearity means that, over the velocity range considered, the loss of kinetic energy per layer is constant. Plots for .22, .30, .45, and .50-caliber projectiles, as shown by Prosser (1988a), confirm this behavior over the initial and a substantial range of velocities. (A reason for the non-zero intercepts is also offered there.) Yet this behavior is in direct contradiction with the data shown in Fig. 6, which implies that the toughness of a yarn (in this case nylon) varies considerably with the strain rate. The explanation offered in Prosser (1988a) was that the plots, although presumed theoretically curved on the basis of the behavior shown in Fig. 6, appear linear because of substantial statistical fluctuations in the V_{50} data. Now, however, a better explanation is available. The energy required to raise the temperature of the yarns in a ballistic panel to the softening point, which is probably at or near the glass transition temperature, depends entirely on the initial temperature distribution in the

panel. If the initial temperature of the panel is uniform, the energy required to raise the temperature of the yarns in any layer to the required softening point is fixed. The yarns simply fail before more heat energy can be generated. Consequently the energy loss per layer should be constant and largely independent of velocity for a given caliber projectile, shape of the leading surface of the projectile, weave, yarn denier, and cloth material used for the ballistic panel as observed. Therefore, the softening/melting phenomena appears to be a major factor in ballistic performance.

The second ramification of the softening/melting phenomena is the relative ballistic performance of nylon and Kevlar. Since the critical velocity for nylon (616 m/s) is higher than that of Kevlar-29 (570 m/s), penetration mechanics based on yarn tensile properties predicts that the ballistic performance of the former should be better. However, the opposite is the case. This implies that yarn tensile and shear properties do not dominate the ballistic performance of the panels at high velocities, and that another variable is involved. Hypothesizing that heat is the additional variable, one would expect to get the relative ballistic performance obtained, since nylon melts when heated whereas Kevlar doesn't melt, but chars.

Tensile and shear properties are important at low ballistic velocities,

MICROSCOPY

Crystallinity changes within Spectra-1000, although exceedingly difficult to observe with TEM, could be seen at much lower resolution, but with greater reliability, by means of polarized LM (Figs 9a,b). Within all fibers subjected to ballistic impact, changes in crystallinity could be

observed by changes in birefringence within test fibers as compared with controls. These changes occur only within several millimeters of the point of impact.

The appearance of five layers of cloth immediately in front of the layer at which the projectile was arrested can be seen in Figs 7a-e. The cloth lay in the path of the projectile and ahead of the layer where the projectile came to rest in the panel. The appearance of the yarns in the penetration path is certainly different from yarns at a distance, even several layers in front of the layer where the projectile stopped, implying a physical change had occurred. The permanent convex shape of the cloth in those layers indicates that the cloth may be heat set, although the indentations might also be due to mechanical deformation. In many cases the cone of indentation for nylon and Spectra was permanent and evident as many as 10 to 12 layers ahead of the layer at which the projectile stopped. In either case, the indentations are evidence that the force of the projectile was felt many layers ahead of its location.

At higher magnifications, molten polymer bridges between yarns can be seen (Figs. 8a-e). The number of bridges decreased significantly from the first layer in front of the projectile to the 5th layer in front and ahead of the projectile. The pattern which the softening/melting seemed to follow was in the shape of a cone with the base (largest area and greatest amount of melting) in layer 1 and the apex (smallest area and least amount of melting) in layer 5.

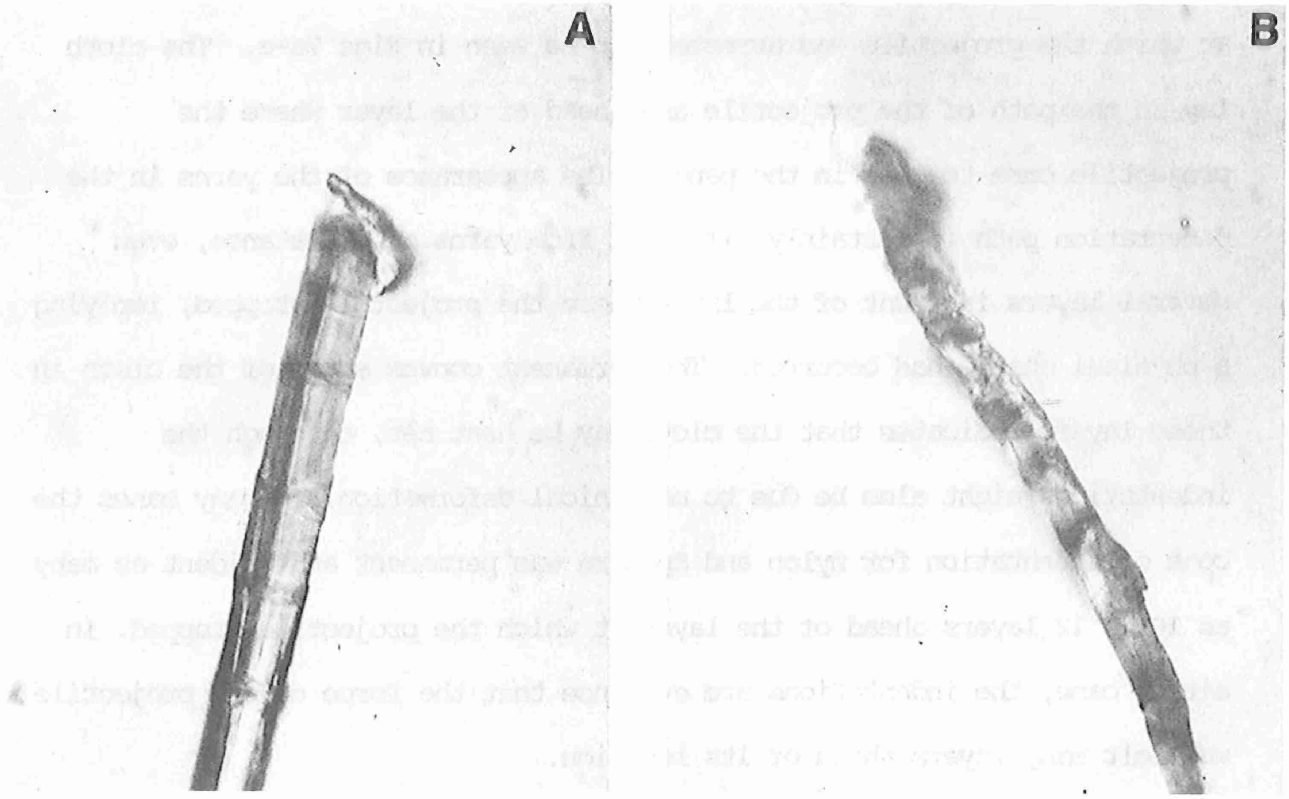

Figure 9. Spectra-1000 - Polarized light micrographs showing A. control undamaged Spectra-1000 filament and B. damaged filament close to point of ballistic impact. Birefringence in B. is indicative of stress induced changes in crystallinity.

X-RAY DIFFRACTION

To determine the phase content, we define X_a, X_m, and X_o to be the mass fractions of amorphous, monoclinic, and orthorhombic phase materials in the specimen, constrained to add up to unity. Our problem is then to calculate two of these mass fractions, using the X-ray diffraction data. Gopalan and Mandelkern (1967) provide a method for determining orthorhombic phase crystallinity in the absence of a monoclinic phase; this method is used to calculate the ratio X_a/X_o in the presence of the monoclinic phase. In this method, a straight line drawn through the Lorenz-polarization corrected data between the experimental intensities at $2\theta = 13^o$ and 27^o is subtracted from the diffraction pattern. Finally, the areas of the crystalline peaks are mathematically separated from the background-corrected curve and denoted A_{001}, A_{110}, and A_{200} for the peaks mentioned above. The amorphous scattering area A_{am} is found by subtracting the three crystalline areas from the total area between 13^o and 27^o for the background-corrected curve.

The amorphous/orthorhombic ratio is found as in Gopalan and Mandelkern by: $R_a = X_a / X_o = A_{am} / (A_{110} + A_{200})$.

Then the monoclinic/orthorhombic ratio is found from the ratio A_{001}/A_{110} using: $R_m = X_m / X_o = K_{fac} (A_{001} / A_{110})$, where K_{fac} is a combined factor for structure factor, multiplicity, and temperature, and has the value 2.074. K_{fac} essentially corrects for the different intrinsic diffraction intensities of the monoclinic (001) and

orthorhombic (110) planes. Once these ratios are known, the three mass fractions are found in three simultaneous linear equations:

$$X_m = R_m X_o$$
$$X_a = R_a X_o$$
$$1 = X_a + X_o + X_m$$

for which the solution is:

$$X_o = 1 / (1 + R_a + R_m)$$
$$X_m = R_m / (1 + R_a + R_m) \text{ and}$$
$$X_a = R_a / (1 + R_a + R_m)$$

The sample data are presented in terms of the disk file name scheme used in data acquisition. Each data pattern identifies the sample, whether penetration is complete or incomplete, and whether a damaged or undamaged zone is being examined. The file name is eight characters, a string which of necessity begins with an alphabetical character, followed by the suffix 0.22, which indicates that $2\theta = 22.00^{o}$ is the center of the pattern. The letter C or I, indicating Complete or Incomplete penetration, is used as the first character. This is followed by the digits identifying a specific test panel sample, then either /D or /U to indicate that the X-ray beam is focused on a Damaged or Undamaged zone, respectively. Table 4 gives a list of the samples and the names of the corresponding patterns.

TABLE 4

Correspondence Between Samples and Diffraction Patterns

		DIFFRACTION PATTERN	
SAMPLE NUMBER	PENETRATION	DAMAGED ZONE	UNDAMAGED ZONE
7-10-1	COMPLETE	C10-1/D.22	C10-1/U.22
7-10-5	COMPLETE	C10-5/D.22	C10-5/U.22
7-10-10	COMPLETE	C10-10/D.22	C10-10/U.22
7-10-15	COMPLETE	C10-15/D.22	C10-15/U.22
7-10-20	COMPLETE	C10-20/D.22	C10-20/U.22
7-10-25	COMPLETE	C10-25/D.22	C10-25/U.22
7-10-30	COMPLETE	C10-30/D.22	C10-30/U.22
7-10-35	COMPLETE	C10-35/D.22	C10-35/U.22
7-5-1	INCOMPLETE	I5-1/D.22	I5-1/U.22
7-5-5	INCOMPLETE	I5-5/D.22	I5-5/U.22
7-5-10	INCOMPLETE	I5-10/D.22	I5-10/U.22
7-5-15	INCOMPLETE	I5-15/D.22	I5-15/U.22
7-5-20	INCOMPLETE	I5-20/D.22	I5-20/U.22
7-5-25	INCOMPLETE	I5-25/D.22	I5-25/U.22
7-5-30	INCOMPLETE	I5-30/D.22	I5-30/U.22
7-5-35	INCOMPLETE	I5-35/D.22	I5-35/U.22

A typical diffraction pattern is shown in Figure 10. The pattern, as shown, has been subjected to the background and the Lorenz-polarization corrections. The vertical scale of the graph is X-ray counts, while the horizontal scale is the Bragg angle 2 . Below the graph the peak search results from the multiple channel analyzer, giving data from the three crystalline peaks (monoclinic [001], and orthorhombic [110], and orthorhombic[200], reading left to right) evident in the pattern. The pertinent data items for each peak are the centroid, the central 2 value of the peak in degrees; the FWHM, or line width (full width half maximum) of the peak in degrees; the peak count above baseline; and the net area of the peak in total counts. (Each peak has been fitted to a Gaussian curve and a baseline; the net area is that of the Gaussian curve.) These net area values are the data used for determination of the mass fractions of the two crystal phases. The amorphous area is found by subtracting the three resolved crystalline areas from the total area of the diffraction curve, indicated under the horizontal axis of Figure 10 with the label A=. The calculated mass fractions of the crystalline and amorphous phases for the patterns are shown in detail in Table 5 and summarized in Table 6.

In the summary (Table 6) the mass fraction data are broken down into four classes for the four combinations of either complete or incomplete penetration, and damaged or undamaged zones. Within each class the average monoclinic and orthorhombic fractions are reported along with their respective standard deviations. Table 6 also includes the results of a replication experiment run to assess the reproducibility of the results.

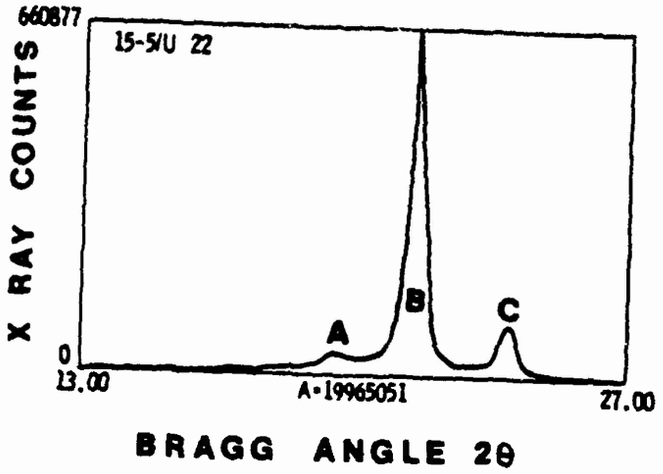

Figure 10. Typical Diffraction Pattern. The diffraction peaks are: A-monoclinic (100); B-orthorhombic (100) and C-orthorhombic (200) The data acquisition time was 1 h 20 min and the area under the curve (in total counts) was 19965051.

TABLE 5

X-Ray Diffraction Showing Monoclinic, Orthorhombic (110) and (200)
Amorphous Content of Spectra-1000 Polyethylene
From Fired Ballistic Panel Fibers*

	Input Areas				Corrected Mass Crystallinities		
Sample	Mono. (001)	Ortho. (110)	Ortho. (200)	Total Area	Mono.	Ortho.	Total (Mono. + Ortho.)
C10-1/D.22	0	11970000	2716000	24060044	0.000	0.610	0.610
C10-1/U.22	261900	9402000	1124000	17024206	0.035	0.606	0.641
C10-5/D.22	0	1274000	223200	3565255	0.000	0.420	0.420
C10-5/U.22	241500	9549000	1431000	16706451	0.034	0.644	0.678
C10-10/D.22	193700	2712000	615200	6384188	0.074	0.498	0.572
C10-10/U.22	204400	9503000	1582000	16958468	0.029	0.643	0.671
C10-15/D.22	2714000	6388000	1444000	14156003	0.047	0.537	0.585
C10-15/U.22	367700	8381000	1401000	16097223	0.054	0.589	0.642
C10-20/D.22	0	1851000	474100	4957032	0.000	0.469	0.469
C10-20/U.22	169800	7690000	1629000	14834582	0.028	0.617	0.646
C10-25/D.22	0	12800000	3505000	27034966	0.000	0.603	0.603
C10-25/U.22	223500	7213000	1022000	13720487	0.038	0.587	0.625
C10-30/D.22	0	7338000	1680000	16757360	0.000	0.538	0.538
C10-30/U.22	124300	7306000	1496000	13238413	0.023	0.656	0.679
C10-35/D.22	435700	3388000	635100	7481225	0.132	0.496	0.628
C10-35/U.22	407300	8035000	1303000	13059411	0.063	0.597	0.660
I5-1/D.22	0	3760000	904400	8971161	0.000	0.520	0.520
I5-1/U.22	206800	8846000	1606000	16501412	0.030	0.623	0.653
I5-5/D.22	672900	8493000	2139000	18541768	0.089	0.542	0.631
I5-5/U.22	414900	10620000	11602000	19965052	0.048	0.595	0.643
I5-10/D.22	158800	4808000	903900	9817222	0.039	0.568	0.607
I5-10/U.22	303700	8821000	1404000	16517419	0.043	0.603	0.647
I5-15/D.22	0	6150000	1512000	13057695	0.000	0.587	0.587
I5-15/U.22	198400	6804000	1142000	12512090	0.038	0.621	0.659
I5-20/D.22	164300	3943000	1048000	8743732	0.048	0.554	0.602
I5-20/U.22	248300	7001000	1106000	12815085	0.045	0.616	0.661
I5-25/D.22	1319000	16830000	4349000	40253760	0.081	0.500	0.581
I5-25/U.22	215500	7471000	1202000	13675321	0.037	0.620	0.658
I5-30/D.22	626200	6618000	1670000	16216661	0.094	0.481	0.576
I5-30/U.22	296000	7155000	1274000	13270735	0.053	0.615	0.668
I5-35/D.22	518900	4211000	785200	9778549	0.121	0.474	0.595
I5-35/U.22	218400	6480000	1140000	12397763	0.042	0.599	0.641

*The amorphous area is found by subtracting the three resolved crystalline areas from the total area of the diffraction curve, indicated under the horizontal axis of Figure 10 with the label A≈. The calculated mass fractions of the crystalline and amorphous phases for the patterns are shown in detail in Table 5 and are summarized in Table 6.

TABLE 6

Summary of

Monoclinic and Orthorhombic Fraction Values

(Table 5)

		MONOCLINIC FRACTION		ORTHORHOMBIC FRACTION	
CLASS	N	AVE.	STD.DEV.	AVE.	STD.DEV.
Complete, Damaged	8	0.032	±0.046	0.521	±0.060
Complete, Undamaged	8	0.038	0.013	0.617	0.025
Incomplete, Damaged	8	0.059	0.042	0.528	0.039
Incomplete, Undamaged	8	0.042	0.006	0.611	0.010
Replicate	5	0.041	0.006	0.613	0.021

For this experiment, a single test specimen (lab sample number 7-5-5, incomplete penetration) was run at five different locations in its undamaged zone. The five different locations were used to assess the sampling effect as well as experimental uncertainty. The results for the replication experiment show a monoclinic fraction of 0.041 (standard deviation 0.006), and an orthorhombic fraction of 0.613 (standard deviation 0.021), for a total crystallinity of 0.654, standard deviation of 0.022.

The results of all of the patterns of undamaged material are in essential agreement at a monoclinic fraction of 0.04 and an orthorhombic fraction of 0.61, with no statistically significant difference between the Complete, Undamaged and Incomplete, Undamaged classes. All undamaged material patterns may be regarded as representative of virgin fabric unaffected by the ballistic impact.

When analyzing the X-ray diffraction data (Table 5) in the damaged classes, two effects are apparent. First of all, the monoclinic fraction shows gross fluctuations from sample to sample, ranging from zero to 0.132. Secondly, the orthorhombic fraction values are lower and show more fluctuation than the undamaged patterns. To illustrate the first effect, in the Complete, Damaged class, five of the eight patterns showed no monoclinic fraction, while the remaining three showed monoclinic fractions of 0.047, 0.074, and 0.132. Illustrating the second effect, orthorhombic fractions in the Complete, Damaged class ranged from 0.420 to 0.610 for the eight patterns.

The changes in phase fractions brought about by the ballistic impact are regarded as arising from very localized heating of the fabric from the kinetic energy of the projectile. This heating can act in two ways. First,

in the range of the well-known alpha transition of 90°C to 100°C, associated with the onset of molecular chain motion in the crystallites, crystallite growth and annealing is possible. Secondly, when the melting point around 140°C is exceeded, polymer will melt, then recrystallize to some extent in the quick cooling process.

For a number of the damaged patterns, evidenced by zero monoclinic content and quite low orthorhombic content, the melting process has predominated. In a few instances, where the monoclinic fraction well exceeds the undamaged value of 0.04, recrystallization or cold working has resulted in further growth of the monoclinic regions, perhaps at the expense of orthorhombic material, whose fraction generally drops with the ballistic event (recall that monoclinic polyethylene arises, generally, in response to mechanical deformation). It is reasonable that in addition to heating and recrystallization, cold working also contributes to changes in phase fractions caused by the ballistic impact, since strains within the filaments themselves are released, thereby contributing to the alterations in the orthorhombic/monoclinic fractions.

Overall, the Complete, Damaged class patterns show lower monoclinic fraction, and more instances of zero monoclinic fraction, than the Incomplete, Damaged class. This is taken to mean that when complete penetration occurs, melting predominates over recrystallization, and indeed is probably associated with the failure of the materials. Recrystallization or cold working or both are evident in the Incomplete, Damaged patterns in the fact that the average monoclinic fraction has increased to 0.059 over the undamaged value of 0.04. The increased scatter in the data for all the damaged patterns is indicative of differences in the ballistic impact event

from one test to the next. While the monoclinic phase serves somewhat as a marker of thermomechanical history, the predominant phase in all patterns is the well-known orthorhombic phase. Both the Complete, Damaged and Incomplete, Damaged classes show significant reduction in orthorhombic content compared to the undamaged fabric.

CONCLUSIONS

1. When counting Spectra-1000 yarns which failed under FSP or RCC impact, under the microscope, numerous yarn ends were observed where the filament ends all lay in, or almost in, a plane and were welded together in the region of the common surface. The fact that all of the severed filament ends were in one surface indicates shearing. No case was found where the filaments were randomly broken along the yarn, typical of a tensile break. The same results were obtained for nylon (Prosser, 1988b). Since the energy loss per layer of cloth (Fig 5 and Prosser 1988a) appears to be largely independent of the velocity for a given caliber projectile, shape of the leading surface of the projectile, weave of the cloth, yarn and filament denier, and cloth material, the major mode of penetration of cloth ballistic panels by projectiles is primarily by rupture of the softened yarns. Consequently, the relative number of tensile vs. shear yarn failures depends on the extent to which the yarns are softened and the relative sharpness of the leading surface of the projectile. The yarn critical velocity may depend primarily on the heat generated on impact.

2. Changes in the birefringence quality of Spectra-1000 fibers as seen by polarized light microscopy provide an excellent qualitative overview of crystallinity changes in fibers subjected to ballistic impact and the observations compare favorably with X-ray diffraction data.

3. Heat-induced polymer bridges between adjacent Spectra-1000 filaments and yarns were observed by SEM in layers ahead of the layer at which the projectile was arrested. As the distance increased ahead of the location where the projectile stopped, fewer bridges were seen.

4. X-ray diffraction data show the following:

a. Undamaged fabric shows an average orthorhombic fraction of 0.61, and an average monoclinic fraction of 0.04.

b. In the damaged fabric, ballistic impact can result in either an increase in monoclinic fraction, attributed to recrystallization, or total eradication of monoclinic material, attributed to melting. The latter predominates where ballistic penetration is complete. This fact implies that the heating effects were more than superficial, i.e., the heat penetrated to the centers of the filaments in the yarn. Some of the heat is obtained from the work of extension. Additional heat may be provided by the projectile via conduction.

c. The major crystalline phase, the orthorhombic phase, is generally reduced in mass fraction by the ballistic impact event in damaged fabric.

d. The monoclinic content of a polyethylene fabric is useful for characterizing thermomechanical effects the fibers have undergone.

REFERENCES

Anonymous. Undated. "Thin Sectioning and Associated Techniques for Electron Microscopy." Dupont/Sorvall Instruments. 3rd Edition. 150 pp.

Anonymous. Encyclopedia of Polymer Science and Engineering. Wiley. 1987, 2nd Edition. 699 pp.

Cullity, B.D. 1956. Elements of X-ray Diffraction. Addison-Wesley. Reading, MA. p 172.

Desper, C.R and R.S. Stein. 1967. Randomization of orientation films and fibers. Polymer Letters. 5:893-900.

Desper, C.R. 1986. An advanced technique for characterization of polymer materials by wide angle x-ray scattering. in Materials Characterization for Systems Performance and Reliability. J.W. McCanley and V. Weiss, eds. Plenum. pp 319-337.

Fatou, J.G, C.H. Baker and L. Mandelkern. 1965. The effects of crystallization conditions and temperature on the polymorphic forms of polyethylene. Polymer. 6:243-248.

REFERENCES

Gopalan, M.R. and L. Mandelkern. 1967. Degree of crystallinity of linear polyethylene from wide-angle x-ray diffraction. Polymer Letters. 5:925-929.

Magill, J.H., S.S. Pollack and D.P. Wyman. 1965. Glass temperature and crystal modification of linear polymethylene. J. Polym. Sci. Pt. A. 3:3781-3786.

Mead, W.T., C.R. Desper and R.S. Porter. 1979. Physical and mechanical properties of ultra-oriented high density polyethylene fibers. J. Polym. Sci., Polym. Phys. Edn. 17:859-892.

Prosser, R.A. 1988a. Penetration of Nylon Ballistic Panels by Fragment-Simulating Projectiles. Part I: A Linear Approximation to the Relationship Between the Square of the V_{50} or V_c Striking Velocity and the Number of Layers of Cloth in the Ballistic Panel. Textile Res. J. 58:61-85.

Prosser, R.A. 1988b. Penetration of Nylon Ballistic Panels by Fragment-Simulating Projectiles. Part II: Mechanisms of Penetration. Textile Res. J. 58:161-165.

REFERENCES

Sawyer, L. 1986. Structure-property relations of liquid crystalline polymers. Proc. Fiber Producer Conf. 5A, 22-24.

Seto, T., T. Hara and K. Tanaka. 1968. Phase transformation and deformation process in oriented polyethylene. Japan. J. Appl. Phys. 7:31-41.

Slichter, W.P. 1956. On the morphology of highly crystalline polyethylenes. J. Poly. Sci. 21:141-148.

Smith, J.C., C.A. Fenstermaker and P.J. Shouse. 1963. Stress-strain relationships in yarns subjected to rapid impact loading. Part X: Stress-strain curves obtained by impacts with rifle bullets. Textile Res. J. November: 33:919-934.

Tanaka, K., T. Seto and T. Hara. 1962. Crystal structure of a new form of high-density polyethylene produced by pressure. J. Phys. Soc. Japan. 17:873-874.

Van Hutten, P.F., C.E. Koning and A.J. Pennings. 1985. The plastic deformation of ultra-high molecular weight polyethylene. J. Mater. Sci. 20:1556-1570.

Weedon, G.C. and T.Y. Tam. 1986. Spectra extended chain polyethylene fibers. Proc. Fiber Producer Conf. 5A, 12-17.

This document reports research undertaken at the US Army Natick Research, Development and Engineering Center and has been assigned No. NATICK/TR-[illegible] in the series of reports approved for publication.